44th AIAA Aerospace Sciences Meeting and Exhibit, 9-12 January 2006, Reno, NV

Property and velocity measurements in a supersonic/hypersonic flow

Martin Boguszko,* Rich Huffman,† and Gregory S. Elliott‡
University of Illinois, Urbana-Champaign, IL 61801

This work presents a non-intrusive laser-based diagnostics technique to measure instantaneous thermodynamic properties and velocity in a compressible fluid flow. The fluid is irradiated with a pulsed narrow-bandwidth Nd:YAG laser at 532 nm. Light scattering from a point in the flow field is collected over a solid angle of about ±20 degrees and focused into a narrow line on an intensified CCD camera using an anamorphic optical system. A molecular iodine filter absorbs the radiation at different degrees with angle thus producing different intensity levels on each pixel along the line. A portion of the light is split and focused on the same CCD chip unfiltered, thus providing an intensity reference from which the fluid density is found. The scattering spectrum and Doppler frequency shift are dependent on the observation angle and fluid properties, and so the values of pressure, temperature and streamwise velocity at every laser pulse using a well-known scattering model.

I. Introduction

THIS work describes a non-intrusive laser-based technique to measure a number of different variables in a flow field by resolving the characteristics of the light scattered from an interrogation point. In the near future the technique will be applied to a closed jet facility capable of achieving supersonic and hypersonic air flow speeds. When operated in a clean and unseeded condition, the Rayleigh scattering from the gas molecules contains information of velocity and the thermodynamic state of the fluid. Additionally tests will be performed with moisture and CO_2 condensation. In this case the technique is capable of resolving velocity only, however a strong increase in signal levels will provide with more accurate results.

The Rayleigh scattering spectrum and intensity from gas molecules is a function of pressure, temperature and the angle of observation relative to the radiant energy direction of propagation as will be shown below. The Doppler frequency shift due to fluid velocity is also a function of observation direction. Shirley and Winter in 1993 devised an arrangement to measure flow quantities by angularly-resolving the filtered Rayleigh scattering.[1] In their work, they proposed an apparatus in which an anamorphic optical collection system with a low f-number was used to collect rays from different scattering angles and record them separately in a linear array of pixels of a CCD camera. Each individual resolution element recorded the scattering subjected to slightly different Doppler shifts, thus obtaining many simultaneous, linearly independent measurement of the same small region. This point-wise technique had the objective of measuring mass flux distributions in the inlet of a high-speed air-breathing propulsion system. Elliott and Samimy[2,3] in 1996 further developed this idea, which they termed filtered angularly-resolved Rayleigh scattering (FARRS), adding to Shirley's arrangement a second and third camera to obtain quantitative average measurements

*Post-doctoral research associate, Dept. of Aerospace Engineering. AIAA member.
†Ph.D. candidate, Dept. of Aerospace Engineering. AIAA senior member.
‡Associate Professor, Dept. of Aerospace Engineering. AIAA associate fellow.

of velocity and thermodynamic properties in an air jet at various running conditions. The work presented here extends this technique to instantaneous measurements.

Successful results of simultaneous density, temperature, and streamwise velocity on a supersonic pressure-matched jet at $M_e = 1.36$ have been obtained. These data were taken with a two-camera arrangement, however, this is currently being modified as will described below so that all this information is captured with a single detector.

II. Theory

The Rayleigh scattering radiation from an unseeded gas can be viewed as having three characteristics: its radiant intensity, the shape of the spectrum, and the frequency shift with respect to that of the incident wave. The intensity of the scattering in a direction φ with respect to the polarization direction[a] is a linear function of the gas number density N and is expressed as.[4]

$$S = \epsilon N L E_i \frac{d\sigma(\varphi)}{d\Omega} \Delta\Omega = R(\varphi) N \tag{1}$$

where S is the grayscale level on the detector, ϵ is a conversion factor that accounts for quantum efficiency (QE) and other optical losses, L is the interrogation path, E_i is the incident radiant energy, $d\sigma(\varphi)/d\Omega$ is the differential cross section, and $\Delta\Omega$ is the solid angle subtended by the collection device. The latter variables can be lumped into a Rayleigh calibration factor $R(\varphi)$ as shown in Eq. (1), which varies as $\sin^2\varphi$, and so the strongest intensity occurs at a scattering angle of $\varphi = \pi/2$. Here the variation with φ is emphasized.

The Rayleigh scattering spectrum from gas molecules $r(x,y)$ can be expressed as a function of two non-dimensional parameters, namely x or the non-dimensional frequency and y or the order parameter and their expressions can be written as[4,5]

$$r = r(x,y) \quad \text{with} \quad x = \frac{2\pi(\nu - \nu_0)}{\kappa a}, \qquad y = \frac{p}{\eta \kappa a} \tag{2}$$

where $(\nu - \nu_0)$ is the optical frequency with respect to the laser central frequency ν_0, $\kappa = 4\pi/\lambda \sin(\theta/2)$ is the magnitude of the wave vector $\boldsymbol{\kappa} = 2\pi/\lambda(\hat{\mathbf{k}}_O - \hat{\mathbf{k}}_L)$ with $\hat{\mathbf{k}}_O$ the scattering direction and $\hat{\mathbf{k}}_L$ the laser direction, λ is the laser wavelength, θ is the scattering angle measured from the laser propagation direction, p is the pressure, η is the shear viscosity of the fluid, and $a = (2kT/m)^{1/2}$ is the most probable molecular velocity, where k is the Boltzmann constant, T is the fluid temperature, and m is the fluid molecular mass.

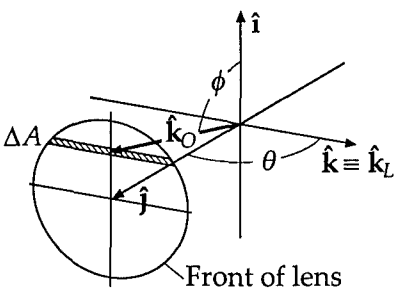

Figure 1. Schematic view of the solid collection angle

The central frequency shift with respect to the incident laser frequency is due to the Doppler effect when the fluid is in motion. The Doppler shift is a function of the orientation of the laser propagation direction and the scattering direction with respect to the flow velocity, and referring to Fig. 1 can be expressed as[6]

$$\Delta\nu_D = \frac{1}{2\pi}\boldsymbol{\kappa}\cdot\mathbf{V} = 1/\lambda\left(\hat{\mathbf{k}}_O - \hat{\mathbf{k}}_L\right) = \frac{1}{\lambda}\left(u\cos\varphi + 0.97v\sin\varphi - w\right) = \Delta\nu_D(\varphi) \tag{3}$$

where u, v, and w are the velocity components, and the factor 0.97 stems from integrating the energy collected through ΔA along the $\hat{\mathbf{k}}$ direction, thus eliminating the θ dependence. From Eq. (3) it is clear that the Doppler shift is different for each viewing angle φ_i over the detection range.

The Doppler shift is detected by placing a molecular iodine filter in front of the detector. The laser is tuned to the mid-point of a steep cutoff edge of a strong absorption feature. Assume for a moment

[a] Assuming that the source of radiation is linearly polarized.

that u is the main velocity component while v and w remain negligible. As the velocity increases, pixels corresponding to angles $\varphi > 0$ will result in $\Delta\nu_0 > 0$ (more radiation is collected), while those imaging angles $\varphi < 0$ will experience $\Delta\nu_0 > 0$ (more radiation is absorbed). The v and w components will change the height and curvature of the resulting signal.

When the radiation is detected by the CCD array it will result as a curve of intensity vs. angle as shown in Fig. If the flow is unseeded density and temperature can also be found. Density is found by collecting the unfiltered scattering while temperature and velocity are coupled and are found together using a non-linear curve-fitting routine. In a seeded flow the signal collected is greatly enhanced, making measurements of velocity more accurate, but thermodynamic information cannot be obtained. A computational algorithm that uses Tenti's S6 model[5] for molecular scattering is used to fit the experimental data has been constructed for particle (PDV) or molecular (FRS) scattering that uses velocity, and velocity, temperature, and density as fitting parameters respectively. Initial results have already been successfully obtained for the unseeded condition and are presented below.

III. Experimental Apparatus

The arrangement that is used in this study is based on the system presented in the work by Elliott and Samimy[2] and the original arrangement by shirley and Winter[1] and is conceptually illustrated in Fig. 2. A pulsed, narrow-bandwidth laser beam with linear polarization along $\hat{\imath}$ and propagating along $\hat{\mathbf{k}}$ is focused into a small interrogation point. A photographic lens with a low f-number (~1.2) collects the scattering over a range of about $\Delta\Omega \approx \pm 20°$. After passing through the field stop the rays are collimated and transformed into a thin line by a spherical-cylindrical lens pair. The rays are divided into two legs, one of which reaches the detector directly while the other is passed through the iodine absorption notch filter before reaching the same detector. The unfilter portion serves as a direct measure of density (in the unseeded running condition) while the filtered portion is used to find velocity (and temperature in unseeded condition). A frequency and laser monitoring system (not shown) is used to normalize small laser fluctuations. The flow is provided by a free air jet exhausting vertically. The detector is an intensified CCD Princeton Instruments camera. Since the signal is photon shot-noise limited the intensifier is expected to greatly enhance the signal levels and also reduce background interference due to its fast-gating capability, and so it is expected to increase measurement accuracy.

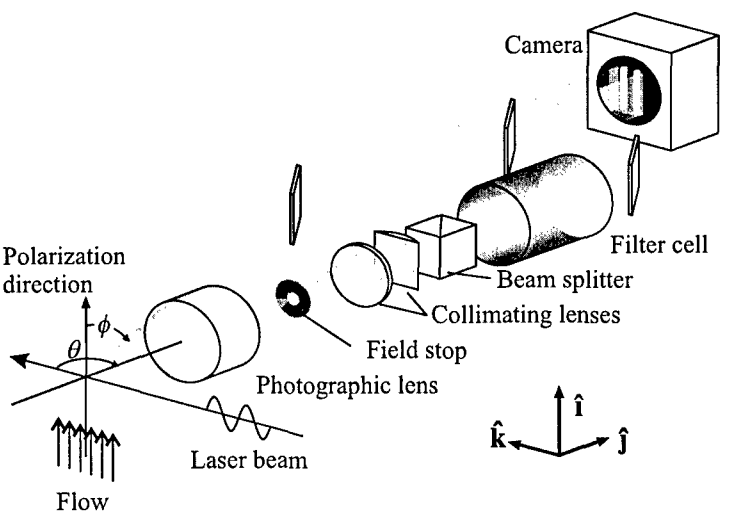

Figure 2. Schematic arrangement of the FARRS experiment

Measurements have been made using a two-camera system with the jet with diameter $D = 12.7\,\text{mm}$ running at designed pressure-matched exit conditions of $M_e = 1.36$ and stagnation temperature of 294 K. The interrogation point was located at a distance of $x/D = 5$ downstream and was traversed radially to 13 different radial locations, starting from the centerline up to $r/D = 2.5$. At every point 700 images were taken, the first and last 100 of which were reference images (no-flow conditions). With every image, values from the laser monitoring system were recorded to determine the laser pulse intensity and optical frequency. The cameras, laser trigger and boxcar integrators were synchronized using a Stanford Research Systems digital delay/pulse generator model DG535.

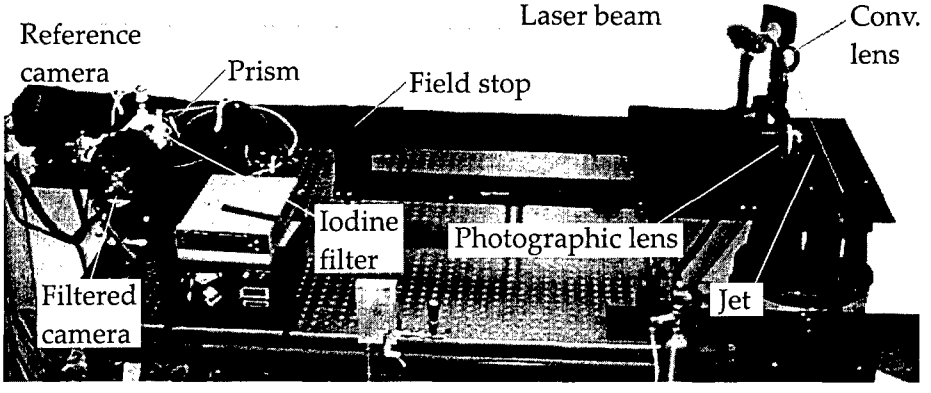

Figure 3. FARRS Experiment layout with two back-illuminated cameras

The total angular range was measured to be $(\pi/2 - 22.5°) \leq \varphi \leq (\pi/2 + 25.4°)$ with an uncertainty of $\pm 0.93°$ and an almost perfectly linear relationship between pixel position and angle. A low-speed coflow around the jet was used to maintain the test region clear of ambient dust particles and condensation. A photograph of the experimental arrangement is shown in figure 3. To reduce background scattering to negligible levels all the light paths were enclosed in black cardboard and the experiment was run in the dark. The cameras used in this case were two 16-bit back-illuminated CCD PixelVision SpectraVideo model SV512 IV (C/A PFT95). Their 512×512-pixel array was used in bin-by-four mode to enhance the signal-to-noise ratio. The signal for both cameras lay in a strip of 23×104 resolution elements. As mentioned above, future runs with a single intensified camera are expected to greatly enhance signal levels and produce better results both in unseeded and seeded conditions. The short-gating capability of the ICCD camera will reduce stray background lighting interference, thus enhancing measurement accuracy.

IV. Test Apparatus

This section describes the equipment and techniques used to gather the FARRS images of a free-shear sonic nozzle experiment performed in July 2005. Figure **??** on page ?? is of the experiment setup, showing the laser beam in green along the light path through the (false color) components, which are labeled and described further in Table **??** on page ??.

The FARRS experiment measured the free shear flow from a nozzle with a measured diameter of 5.077 mm. The nozzle was pointed vertically with flow exiting upward. To analyze the flow properties at different locations, the laser beam and receiver optics were held fixed and the nozzle was repositioned by means of a computer-controlled, three-axis gear drive table. The collimated light source was a Spectra Physics Quanta Ray laser, model number GCR-230. The beam produced was a 8 ns long pulse, repeating at 10 Hz, producing a 650 mJ pulse. The laser pulse wavelength was nominally 532.20 nm, adjustable by ± 0.01 nm (or ± 8.7 GHz) and vertically polarized. The beam was turned by a dichroic mirror and focused to a point just

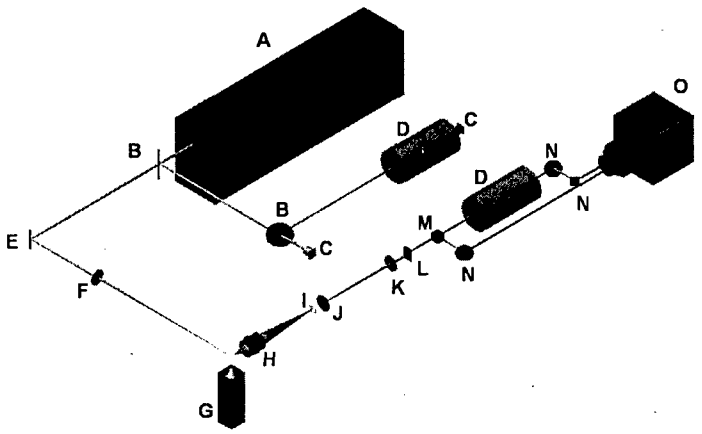

	Description
A	Spectra Physics Quanta Ray GCR-230 Nd:YAG Laser
B	Beam Splitter
C	ThorLabs Det 210 Photodiode
D	Iodine Cell
E	Dichroic Mirror
F	Speherical Lens, f 500 mm
G	Test Nozzle, 5.077 mm, Flow Vertically Upward
H	Nikkor S.C 50 mm Camera Lens
I	ThorLabs ID-12 Iris, Field Stop
J	Sherical Lens, f 500 mm
K	Sherical Lens, f 500 mm
L	Cyliderical Lens, f 1000 mm
M	Non-poloarizing Prismatic Cube 25.4 mm $\frac{1}{4}$ wave
N	Silver Coated Mirror
O	Princeton Instruments ICCD-576-S Intensified Charge-Coupled Device Camera, 384×576 pixels

Figure 4. Average temperature contours of low-speed jet at different stagnation temperatures

beyond the interrogation region to prevent camera damage. The power produced by the laser pulse after being focused to a point is capable of igniting dust particles. If the light emitted by reaction with a dust particle was allowed to enter the camera, camera damage would occur. Additionally, the focusing lens was turned off axis to prevent constructive interference from ionizing air in the interrogation region.

As the beam exited the laser cavity, it was split with a dichroic mirror. One path provided an interrogation light source and is discussed later. The other path was split further by a second dichroic mirror to determine the pulse intensity and frequency. The first branch of the beam was sent directly to a photodiode to measure pulse intensity. The voltage signal converted from the photodiode was sent to a boxcar integrator and the result was recorded for each pulse. The second branch of this beam was sent through an iodine cell and then into a photodiode and integrated through another boxcar integrator. The iodine cell contained a known number density of iodine which was set by the vapor pressure of an iodine crystal released into the evacuated cell. The number density was verified by a calibration in which the laser swept through its frequency range and the photodiode output was recorded and compared to the theoretical absorption spectrum based on frequency and number density. The laser frequency was adjusted to be centered at the midpoint of absorption on a specific location in the absorption spectrum (532.20 nm or 563.3065THz). Minor pulse-to-pulse variations in frequency were then determined based on the relative intensity between the two integrated photodiode signals.

It is important to note, the laser provides tunable frequency by means of a small, internal seed laser. After the experiment was completed, the laser seeder was diagnosed as being out of tolerance. The symptom of concern to this experiment was the acquisition of unseeded pulses in the data. An unseeded pulse did not contain a Gaussian frequency distribution. The spectrum covered by an unseeded signal is much broader than the normal, seeded signal. This broader spectrum sent significant energy around the rather narrow absorption notch in the iodine cell. Errors occurred in determining pulse frequency and flow properties when the interrogation beam was unseeded. Although most of the pulses recorded were seeded, unseeded images were recorded in the data. A discriminator for eliminating all unseeded pulses was not discovered. This experiment is planned to be repeated with the repaired laser.

The Raliegh scattering optical signal was received by a Nikkor S.C 50 mm camera lens, with the aft end (the end which mates normally to the camera body) of the lens pointed toward the nozzle. The image was focused to a point and passed through a field stop to block the signal received out of the interrogation region. Downstream of the field stop, the image was collimated with a spherical lens and then focused to a line through a cylindrical lens. The linearly focused beam was aligned vertically with the flow to provide angular resolution in the primary direction of flow. Then the beam was split through a cube prism and sent

down two paths. The first path sent the beam through a calibrated iodine cell and was focused onto the image intensified charge-coupled device (CCD) camera. The second path was routed around the iodine cell by three silver-coated mirrors and focused onto the same CCD, directly adjacent to the iodine cell filtered image. The camera was synchronized with the pulse train of the laser and recorded images at 3 Hz. The images not recorded by the camera were discarded.

V. Data Reduction

Each image was evaluated for particles in the flow. The relative intensity of the camera image with embedded particles (e.g. dust, oil) was roughly an order of magnitude higher than an image free of such particles (as measured by a simple summation of pixel intensities). Images above a predetermined threshold were eliminated from the data set. The threshold was determined by visual inspection of the images. Most particle images illuminated large portions of the CCD (areas outside of the nominal lines regions) and were recognizable visually. After initial segregation, it was noted that a small number of particle images were still included in the data, estimated at around 5% (visual inspection was used, but a quantitative measure was not found). A technique to eliminate these particle laden images was not found. This experiment was accomplished using a house air supply with a high number of particles. A filter was placed inline before the nozzle and particle count was reduced significantly (reduced from over 72% particle images captured to 10%). This experiment will be repeated in the future using a separate air supply to reduce the particle count further.

After initial parsing, the images were reduced to two lines of intensity versus image angle. The images were calibrated for angle by means of a knife edge placed in front of the camera lens and traversed vertically across the face of the lens. A mapping of image pixels to angle was produced from this calibration and applied to the flow images. The collapsed image lines were then compared to an image taken with known flow conditions (jet turned off, pressure and temperature measured). Density was determined directly from relative image intensity which is proportional to air molecule number density in the interrogated flow volume. The flowfield variables of velocity, temperature, and pressure were determined by means of non-linear Levenberg-Marquardt curve-fitting algorithm developed by Boguszko (ref 999) for each image taken. The algorithm was implemented in MATLAB and run against the experimental data. The results of this processing showed mean values which correlate well to isentropic predictions (and will be discussed further in the next section). However, the standard deviation of the results was on the order of the data. To eliminate spurious results, calculations which yielded values which were more than 1 standard variation away from the average in the calculated parameters of: pressure, temperature or velocity were eliminated from the dataset after calculations were complete. These discarded data were attributed to unseeded laser signals or particles in the interrogated flow volume, which sent the curve-fitting algorithm to wildly erroneous results.

Figure 5 on the following page shows the interogation stations of the jet flowfield. In the center of the flow, stations were spaced every 1 mm, centered on the nozzle. Additional points surround the inner stations to ensure the edge of the wake was determined.

Additionally, a variation to the experiment was accomplished. In the varied technique, moisture already present in the compressed air source was used as a seed particle to extract doppler information from the flow. The Raleigh scattering signal was dwarfed by the doppler return and eliminated the possibility of determining density, pressure or temperature in the flow.

VI. Results

On the unfiltered side, the ratio of flow vs. no-flow images removes the optical calibration constants resulting in a measurement of flow density. With this result and the ratio flow vs. no-flow of filtered images the optical constant are also removed and the resulting data are only a function of thermodynamic

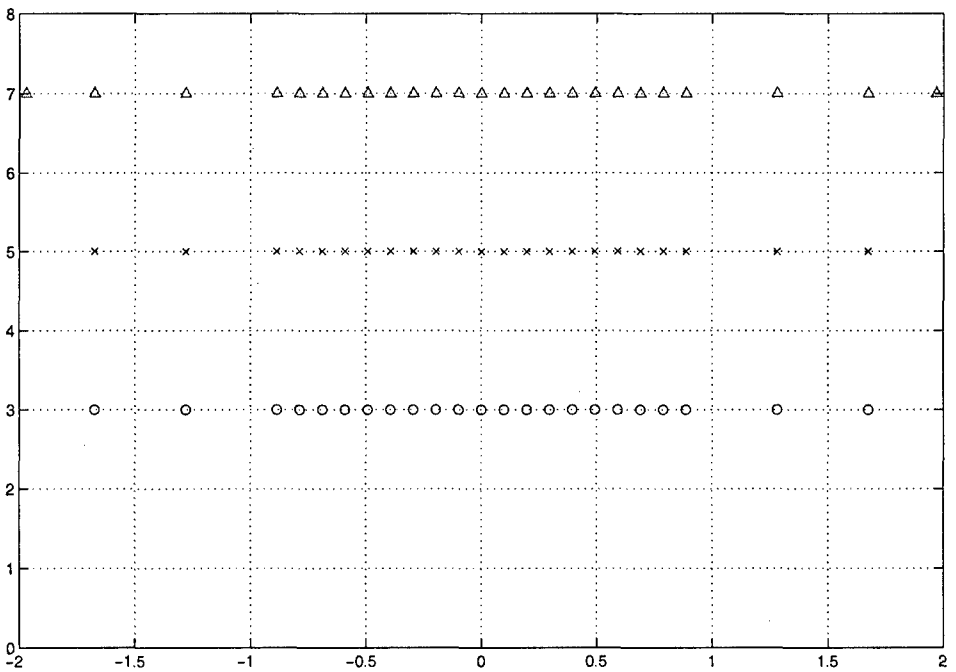

Figure 5. Interrogation Stations of the Jet Flowfield.

properties and velocity. Figure 6 shows an example of the normalized data points collected at a single exposure (open symbols), superimposed with the curve fit of the FARRS model (closed symbols). This non-linear curve fitting requires an initial guess. The system converged to the expected solution when ambient conditions were given as the starting guess, except at few isolated points which were discarded from the analysis. It is important to note that an important assumption was made, namely that the streamwise velocity component is dominant, thus only the first term in Eq. (3) was considered.

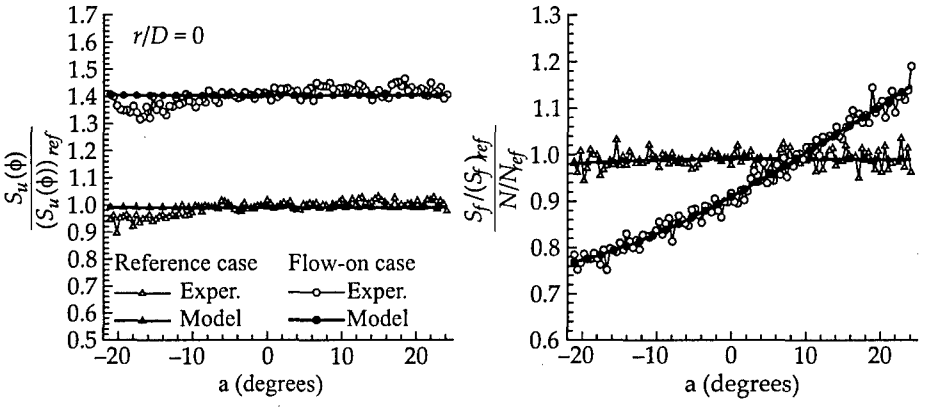

ρ_{ref}= 1.20±0.008 kg/m^3
ρ = 1.64±0.006 kg/m^3

a. Density calculation

u_{ref} = 1.80±3.47 m/s
u = 468.4±43.1 m/s
T_{ref}= 300.8±0.7 K
T = 261.9±9.0 K

b. Temperature and velocity calculation

Figure 6. Sample solution at reference conditions (jet off) and at running conditions (jet on) using the Levenberg-Marquardt non-linear curve-fitting routine with ρ, u, and T as fitting parameters

This process is repeated frame by frame, obtaining instantaneous results for each one, which allows the technique to be applied to unsteady and compressible turbulent flows. Average thermodynamic properties were also compared to theoretical isentropic values in the core of the jet, since the nozzle exit was pressure-matched. Although isentropic conditions are supposed to exist at the exit, discrepancies of the values measured at $x/D = 5$ are below 9%. This is is due to the low spreading rate of shear layers in supersonic flows.

Table 1. Comparison of measured quantities with respect to theoretical isentropic values within the jet core

	Measured	Isentropic	Rel. Diff.
u (m/s)	364	399	-8.9%
ρ (kg/m^3)	1.57	1.65	-4.8%
T (K)	223	215	3.7%

Although laser Doppler velocimetry (LDV) has a higher data acquisition rate, it does not capture thermodynamic quantities, since it requires artificial seeding. Average and RMS velocity values were compared to LDV measurements published by Mosedale.[7] In figure 7.a the radial values of velocity from FARRS and LDV are compared. The agreement of the two techniques is quite good with the FARRS mean velocity at the jet core being approximately 5% to 7% below the LDV results. At the shear layer RMS velocity values are about 25% higher than those obtained by LDV, and it is believed to be due to the assumption that the Doppler shift is solely due to streamwise velocity. Figure 7 also shows the curves corresponding to the average and RMS results for each property as a function of radius. The correct trends are observed, where the velocity decreases as we move farther from the center line, the density

decreases and the temperature increases to ambient conditions.

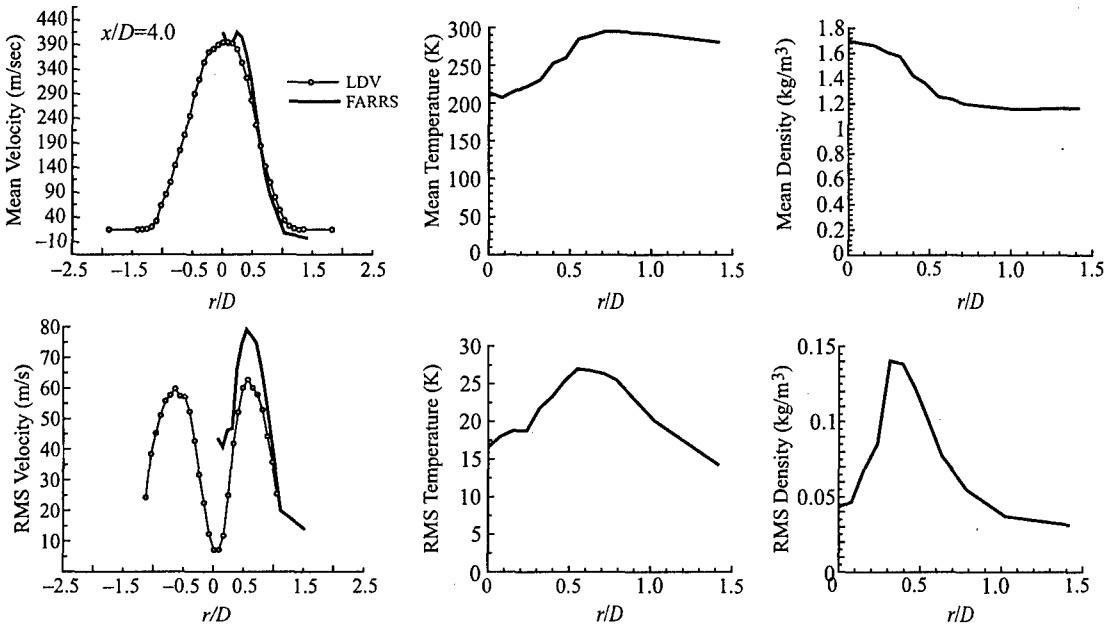

Figure 7. Curves of streamwise velocity, temperature, and density as a function of radius

Figures 8 parts (a) through (c) show the mean profiles for flow speed, density, and temperature, respectively. Results from the center of the jet match the isentropic predictions well, and the core of the jet expands and decelerates as it travels downstream. For a converging jet expanded isentropically to local atmospheric conditions, Table 2 on the following page delineates the predicted results of the flow parameters. The fluctuating parameters were an order of magnitude higher than predictions and did not accurately describe the turbulent wake. The fluctuating parameters will be investigated further in experiments using a cleaner air supply beginning in 2006.

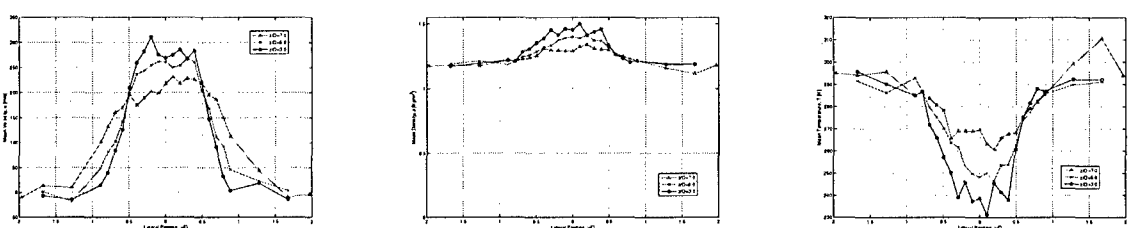

(a) Flow Speed (b) Density (c) Temperature

Figure 8. Mean Flow FARRS Results, Mach 1.0 Converging Nozzle at Multiple Downstream Locations

Figure 9 on page 11 parts (a) and (b) are the mean and fluctuating results of a Mach 1.36 jet (nominally 400 m/s) using condensation seeding with the Iodine filter setup. The mean data compare acceptably to the original experiment by Boguszko using the same nozzle and flow conditions (?). However, the fluctuating data show a shift of 70m/s over the earlier experiment. It is believed the fluctuations are biased by noise from poor laser seeding quality and particles in the flow.

Table 2. Isentropic Jet Predictions

Parameter	Value
Density, ρ	1.43 Kg/m^3
Temperature, T	242.3 K
Velocity u	312.2 m/s

VII. Conclusion

Initial results from the jet running in unseeded condition are very encouraging since they verify that the numerical processing algorithms are consistent with the scattering process. However the model will have to looked at closer to fully understand the reason that the RMS velocity results are higher than previously reported by other investigators. The use of the intensified camera in the near future will help resolve the other two velocity components (assumed negligible here), and so it will be possible to remove the streamwise-only velocity assumption thus providing a more accurate picture of the flow behavior. Runs at different conditions with and without condensation seeding will be run and the results along with their corresponding accuracy analysis will be presented at the time of the presentation of this paper.

References

[1]Shirley, J. A. and Winter, M., "Air-mass flux measurement system using Doppler-shifted filtered Rayleigh scattering," *AIAA Paper No. 93-0513*, 1993.

[2]Elliott, G. S. and Samimy, M., "Rayleigh scattering technique for simultaneous measurements of velocity and thermodynamic properties," *AIAA Journal*, Vol. 34, No. 11, 1996, pp. 2346–2352.

[3]Elliott, G. S. and Samimy, M., "A molecular filter based technique for simultaneous measurements of velocity and thermodynamic properties," *AIAA Paper 96-0304*, 1996.

[4]Seasholtz, R. G., Buggele, A. E., and Reeder, M. F., "Flow measurements based on Rayleigh scattering and Fabry-Perot interferometer," *Optics and lasers in engineering*, Vol. 27, 1997, pp. 543–570.

[5]Tenti, G., Boley, C., and Desai, R., "On the kinetic model description of Rayleigh-Brillouin scattering from molecular gases," *Canadian Journal of Physics*, Vol. 52, 1974, pp. 285–290.

[6]Drain, L. E., *The Laser Doppler Technique*, John Wiley and Sons, New York, 1980.

[7]Mosedale, A. D., *An Investigation of the Planar Doppler Velcimetry Technique*, Master's thesis, Rutgers University, New Brunswick, New Jersey, 1998.

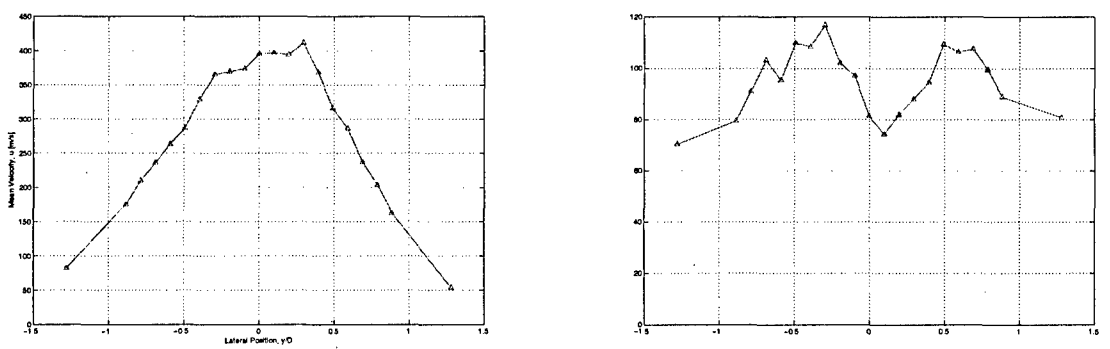

(a) Mean Flow Speed

(b) Fluctuating Flow Speed

Figure 9. Moisture-Seeded Doppler Results, Mach 1.36 Converging Nozzle at $z/D = 7.0$

JAN 13 2006

REPORT DOCUMENTATION PAGE	Form Approved OMB No. 0704-0188

1. AGENCY USE ONLY *(Leave blank)*	2. REPORT DATE	3. REPORT TYPE AND DATES COVERED
	9.Jan.06	MAJOR REPORT

4. TITLE AND SUBTITLE
PROPERTY AND VELOCITY MEASUREMENTS IN A SUPERSONIC FLOW.

5. FUNDING NUMBERS

6. AUTHOR(S)
MAJ HUFFMAN RICHARD E JR

7. PERFORMING ORGANIZATION NAME(S) AND ADDRESS(ES)
UNIVERSITY OF ILLINOIS AT URBANA

8. PERFORMING ORGANIZATION REPORT NUMBER
CI04-1722

9. SPONSORING/MONITORING AGENCY NAME(S) AND ADDRESS(ES)
THE DEPARTMENT OF THE AIR FORCE
AFIT/CIA, BLDG 125
2950 P STREET
WPAFB OH 45433

10. SPONSORING/MONITORING AGENCY REPORT NUMBER

11. SUPPLEMENTARY NOTES

12a. DISTRIBUTION AVAILABILITY STATEMENT
Unlimited distribution
In Accordance With AFI 35-205/AFIT Sup 1

12b. DISTRIBUTION CODE

13. ABSTRACT *(Maximum 200 words)*

DISTRIBUTION STATEMENT A
Approved for Public Release
Distribution Unlimited

14. SUBJECT TERMS	15. NUMBER OF PAGES
	11
	16. PRICE CODE

17. SECURITY CLASSIFICATION OF REPORT	18. SECURITY CLASSIFICATION OF THIS PAGE	19. SECURITY CLASSIFICATION OF ABSTRACT	20. LIMITATION OF ABSTRACT

THE VIEWS EXPRESSED IN THIS ARTICLE ARE THOSE OF THE AUTHOR AND DO NOT REFLECT THE OFFICIAL POLICY OR POSITION OF THE UNITED STATES AIR FORCE, DEPARTMENT OF DEFENSE, OR THE U.S. GOVERNMENT.